# Anderson disorder-induced nontrivial topological phase transitions in two-dimensional topological superconductors

Hai-Bin Wu[1] and Jian-Jun Liu[1,2,*]

[1]*College of Physics, Shijiazhuang University, Shijiazhuang 050035, China*
[2]*College of Physics, Hebei Normal University, Shijiazhuang 050024, China*

We numerically investigate the quantum phase transitions induced by Anderson disorder in a topological superconductor (TSC), which is composed of a quantum anomalous Hall insulator (QAHI) and a proximity coupled $s$-wave superconductor (SC). From the transport phenomena presented, we deduce that with the increase of Anderson disorder strength, the topological quantum phase changes from Chern number $\mathcal{N} = 0$ to $\mathcal{N} = 1$ and finally to $\mathcal{N} = 2$. Then we use the effective-medium theory to verify our numerical results and conclude that the phase transitions should ascribe to the negative correction of topological mass.

## I. INTRODUCTION

Majorana fermions, which are their own antiparticles [1] and obey exotic non-Abelian statistics, may play a crucial role in future fault-tolerant topological quantum computation [2–4]. Finding such particles is a wide concern topic in the fields of condensed matter physics and material science. Since they are most likely to exist in topological superconductors (TSCs), TSCs become one of the most fascinating fields nowadays [5–8]. These particles, which exist in the form of quasiparticles in the condensed matter system, were first predicted to be found in the fractional quantum Hall state [9,10]. Subsequently, in 2000, Read and Green theoretically predicted that Majorana fermions would appear in a $p_x + ip_y$ wave superconductor (SC) [11]. In 2001, Kitaev proposed a simple one-dimensional toy model for spinless $p$-wave SC. He also proved that Majorana fermions appear at both ends of this one-dimensional SC [12]. Since the proposed SC is difficult to realize in experiment, it has not attracted many people's attention. The discovery of topological insulator (TI) provides an ideal research platform for Majorana fermions. In 2008, Fu and Kane pointed out that the proximity effect between normal $s$-wave SC and the surface states of a strong TI can result in the generation of $p_x + ip_y$ wave TSCs and the Majorana fermions can appear at the interface between the TI and the SC [13,14]. Henceforward, researches on the TI in the proximity of a SC have attracted extensive attention from many researchers [15–20].

Recently, Chung *et al.* [21] and Wang *et al.* [22] theoretically predicted that the two-dimensional (2D) chiral TSC state can be realized in the quantum anomalous Hall insulator (QAHI) thin film through the proximity effect to a conventional $s$-wave SC. The unique signature is that the longitudinal conductance is quantized into a half-integer conductance plateau with a value of $e^2/2h$ in their hybrid structure. In

2017, He *et al.* have observed such a quantized plateau experimentally in the QAHI bar covered by the $s$-wave SC, which is signature of chiral Majorana fermion [23]. However, Ji *et al.* [24] indicated that the observed half-integer conductance plateau may not imply the existence of one-dimensional chiral Majorana fermions. They claimed that a metallic phase in the central region of hybrid structure also presents a quantized conductance of $e^2/2h$. Almost simultaneously, based on the percolation theory Huang *et al.* [25] found the existence of a similar conductance plateau in the magnetic disordered hybrid structure at a relatively high temperature or in the presence of dephasing arising from the interplay of disorder and temperature [26]. Subsequently, Lian *et al.* [27] theoretically compared the critical behavior near the $e^2/2h$ conductance plateau induced by the TSC with the conductance plateau predicted by Huang *et al.* and finally pointed out that the two plateaus can be distinguished in the experiment. In 2020, Kayyalha *et al.* experimentally studied similar QAHI-SC hybrid devices; they found that the half-quantized conductance plateau is unlikely to be induced by chiral Majorana fermions in their samples with a highly transparent interface [28]. Therefore, one may ask: What are the characteristics of the quantized conductance of $e^2/2h$ induced by disorder? More importantly, what is the physical mechanism of the quantized conductance of $e^2/2h$? These questions still need to be clarified.

The defects are an inevitable factor in manufacturing processes. Moreover, the effect of disorder constitutes a crucial issue in the unique transport properties of the topological materials being studied. Therefore, various topological systems exhibit many novel phenomena induced by disorder [29–35]. The most striking of these phenomena is the phase transition of TI caused by the strong disorder, which discovered the topology Anderson insulator [35]. Then, by using the effective-medium theory, Groth *et al.* theoretically demonstrated the physical mechanism of this topological quantum phase transition induced by Anderson disorder [36]. Based

————————
*liujj@hebtu.edu.cn

on this theory, Song *et al.* and Guo *et al.* discussed the phase transition in a 2D TI system with different disorder [37] and a three-dimensional TI system with nonmagnetic disorder, respectively [38]. TSC is another topological matter discovered after the TIs. The TSC hybrid structure involving Majorana fermions exhibit extraordinary physical phenomena in transport, especially for the clean $\mathcal{N} = 1$ chiral Majorana edge case, which presents four scattering processes: transmission, local Andreev reflection, crossed Andreev reflection, and normal reflection. These four processes have equal probability with a value of 0.25 [16,21]. Recently Mross *et al.* [39] and Wang *et al.* [40] predicted that disorder can induce transition between the non-Abelian phase and Abelian phase, resulting in changes of the thermal Hall conductance plateau. Before these reports, Ryu and Nomura have pointed out that disorder not only induces topological quantum phase transition in TI but also in TSC [41]. Subsequently, Borchmann *et al.* used three different methods to find evidence for the change of Chern number with Anderson disorder in spin-orbit coupled TSC, which is named Anderson TSC [42]. The phase transitions from high Chern number phase into a topological phase with Chern number $\mathcal{N} = 1$ is seen in all of their three cases. Investigating the effects of disorder on the one-dimensional dimerized Kitaev superconductor chain by using the Su-Schrieffer-Heeger model, Hua *et al.* found that the phase transition can also occur [43]. Before that, Qin *et al.* theoretically explored the effects of disorder on the topological phases in 2D Rashba spin-orbit coupled SC. They found that a topologically trivial TSC can be driven into a nontrivial chiral TSC upon diluted doping of isolated magnetic disorder [44]. However, it is still unclear whether Anderson's disorder can induce a trivial quantum phase in 2D TSC to a nontrivial quantum phase, as TI does.

Thus in this paper, we study 2D QAHI proximity coupled by an *s*-wave SC in a hybrid system where Anderson disorder in the central top-covered region is considered, as shown in Fig. 1(a). It is found that between the $\mathcal{N} = 2$ phase and $\mathcal{N} = 0$ phase, there is a topological quantum phase with $\mathcal{N} = 1$. The result is similar to the work of Lian *et al.* [27]. In their work, they claimed that the disorder induced by the magnetic field can cause the change of Chern number in TSC. But we find that in our model, with the increase of nonmagnetic Anderson disorder strength, the topological quantum phase changes from $\mathcal{N} = 0$ to $\mathcal{N} = 1$ and finally to $\mathcal{N} = 2$. Based on effective-medium theory, we further calculate the renormalized topological mass. The calculation results show that the topological mass obtains a negative correction with the increase of disorder strength. More specifically, the trivial TSC phase represented by point B in the phase diagram [see Fig. 1(b)] can be driven into the chiral TSC phase [blue region in Fig. 1(b)]. Therefore, we come to the conclusion that Anderson disorder can adjust the magnetic strength, resulting in closing and reopening the band gap of TSC.

This paper is organized as follows: In Sec. II, our theoretical model and used approach are introduced. In Sec. III, disorder induced topological phase transition is discussed. In Sec. IV, mechanism and explanation of the topological phase transition are given. Finally, in Sec. V a brief conclusion is summarized.
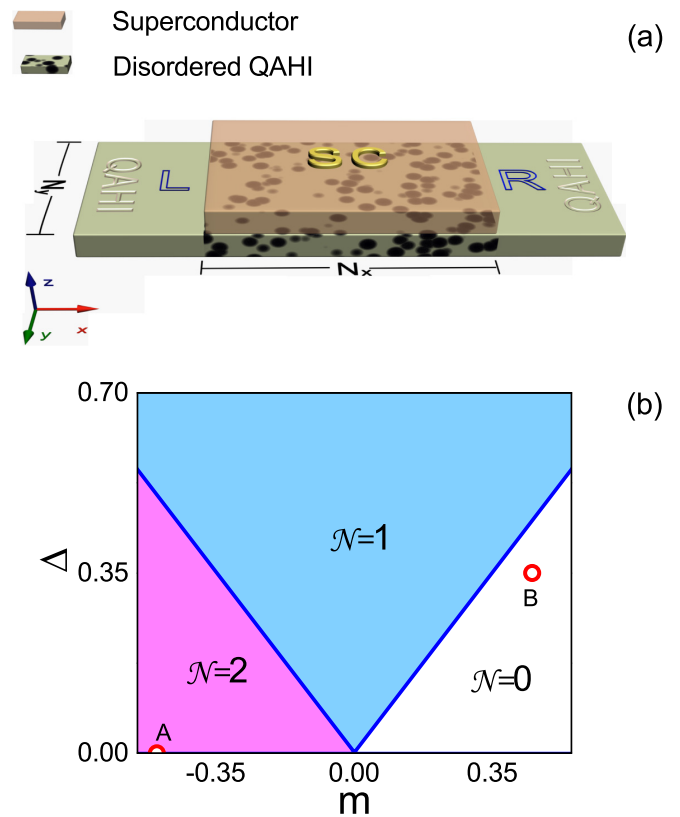


FIG. 1. (a) Schematic diagram of the QAHI/TSC(trivial)/QAHI hybrid system. The labels L and R refer to the corresponding leads. The dirtied central region represents the nontrivial TSC region where disorder is applied in the calculations. (b)Phase diagram of the TSC in the $(\Delta, m)$ plane for $\mu = 0$. Red hollow circles A and B denote the phase point in the two leads and in the central trivial TSC region used in the calculation, respectively. $\mathcal{N}$ label the Chern number of the TSC. Here, only $\Delta > 0$ are given.

## II. MODEL AND METHOD

We consider a QAHI/trivial TSC/QAHI hybrid structure that couples an *s*-wave SC to the disordered central region of a QAHI film, as shown in Fig. 1(a). The size of the central region is $N_x \times N_y$. Given a basis of the $k$ space $[c_\uparrow(k), c_\downarrow(k)]^T$, where $c_\uparrow(k)$ ($c_\downarrow(k)$) is the annihilation operator, $\uparrow$ ($\downarrow$) represents spin-up (spin-down). In our numerical calculation, we adopt the most general two-band Hamiltonian with low-energy effective states near the $\Gamma$ point describing the 2D QAHI system, which can be expressed in the following form [45,46]:

$$H_{\text{QAHI}}(k) = \begin{pmatrix} m + Bk^2 & A(k_x - ik_y) \\ A(k_x + ik_y) & -m - Bk^2 \end{pmatrix}, \quad (1)$$

where $A$, $B$, and $m$ are material parameters. Since we use the nearest-neighbor tight-binding representation in the calculations, the corresponding Hamiltonian of a 2D square lattice can be obtained by Fourier transformation. Therefore, the Hamiltonian in equation (1) can be expressed

as [47]

$$H_{\text{QAHI}} = \sum_i \varphi_i^\dagger T_0 \varphi_i + \sum_i \varphi_i^\dagger T_x \varphi_{i+\delta x}$$
$$+ \sum_i \varphi_i^\dagger T_y \varphi_{i+\delta y} + \text{H.c.},$$

$$T_0 = (m + \frac{4B}{a^2})\sigma_z,$$

$$T_x = -\frac{B}{a^2}\sigma_z - \frac{iA}{2a}\sigma_x,$$

$$T_y = -\frac{B}{a^2}\sigma_z - \frac{iA}{2a}\sigma_y, \quad (2)$$

where $i$ represents the real space coordinate site $(x, y)$, $\delta x$ ($\delta y$) is the unit vector along the $x$ ($y$) direction, $\varphi_i = [c_{i\uparrow}, c_{i\downarrow}]^T$ are annihilation operators of the electron on site $i$ in real space for spin-up and spin-down, $\sigma_{x,y,z}$ are the Pauli matrices, and $a$ is the lattice constant.

The Bogoliubov-de Gennes (BdG) Hamiltonian of QAHI proximity coupled with an $s$-wave SC in the central region is

$$H_{\text{TSC}}(k) = \begin{pmatrix} H_{\text{QAHI}}(k) + \mu & i\Delta\sigma_y \\ -i\Delta^*\sigma_y & -H_{\text{QAHI}}^*(-k) - \mu \end{pmatrix}, \quad (3)$$

where potential energy of the top-gated voltage in central TSC region is represented by $\mu$ and the basis vector is expressed by $\varphi_k = [c_\uparrow(k), c_\downarrow(k), c_\uparrow^\dagger(k), c_\downarrow^\dagger(k)]^T$. $\Delta$ is induced pairing potential due to the proximity to an $s$-wave SC.

We include the effects of Anderson disorder by adding an onsite potential term; by considering particle-hole symmetry, the Anderson disorder of TSC in real space is described by the Hamiltonian [47],

$$H_D = \sum_i \psi_i^\dagger w_i \tau_z \otimes \sigma_0 \psi_i, \quad (4)$$

where $w_i$ is the onsite disorder energy uniformly distributed in the range $[-W/2, W/2]$ with the disorder strength $W$. $\psi_i = [c_{i\uparrow}, c_{i\downarrow}, c_{i\uparrow}^\dagger, c_{i\downarrow}^\dagger]^T$ is the spinor on site $i$ in Nambu space. $\tau_z$ is the Pauli matrix in the $z$ direction acting on the particle and hole degrees of freedom, and $\sigma_0$ denotes the unit matrix in spin space.

With the aid of the Keldysh nonequilibrium-Green-function technique, a formal expression for current from the left ($L$) or right ($R$) lead to the central region can be written as [48,49]

$$I(E) = \frac{ie}{\hbar} \int \frac{dE}{2\pi} Tr\{\Gamma^{L/R}(E)(G^<(E)$$
$$+ f_{L/R}(E)[G^r(E) - G^a(E)])\}, \quad (5)$$

where $G^r(E) = [G^a(E)]^+ = (E - H_{\text{TSC}} - \Sigma_L^r - \Sigma_R^r)$ is the retarded (advanced) Green's function of central TSC region in Nambu representation. The broadened $\Gamma^{L/R}$ is defined as $\Gamma^{L/R}(E) = i[\Sigma_{L/R}^r - \Sigma_{L/R}^{r+}]$. $\Sigma_{L/R}^r$ is the retarded self-energy due to the coupling between $L$ ($R$) lead and central TSC region [50–53]. $f_{L/R}$ represents the Fermi distribution function in the $L$ ($R$) lead. Considering the condition that electron and hole in the two leads are not coupled, we divide each quantity of equation (5) under the Nambu representation into two parts,

electron and hole. we obtain

$$I(E) = \frac{e}{h} \int dE Tr\{(f_{Le} - f_{Rh})\Gamma_{ee}^L G_{ee}^r \Gamma_{ee}^R G_{ee}^a$$
$$+ (f_{Le} - f_{Rh})\Gamma_{ee}^L G_{eh}^r \Gamma_{hh}^R G_{he}^a$$
$$+ (f_{Le} - f_{Lh})\Gamma_{ee}^L G_{eh}^r \Gamma_{hh}^L G_{he}^a\}, \quad (6)$$

where $G^{r/a} = \begin{pmatrix} G_{ee}^{r/a} & G_{eh}^{r/a} \\ G_{he}^{r/a} & G_{hh}^{r/a} \end{pmatrix}$, $\Gamma^{R/L} = \begin{pmatrix} \Gamma_{ee}^{R/L} & 0 \\ 0 & \Gamma_{hh}^{R/L} \end{pmatrix}$. $e(h)$ indicates electron (hole). $f_{Le/Lh}$ ($f_{Re/Rh}$) represents the electron or hole Fermi distribution function of the $L$ ($R$) leads. Thus the transmission coefficient ($T$), Andreev reflection coefficient ($T_{\text{AR}}$), and cross Andreev reflection coefficient ($T_{\text{CAR}}$) can be obtained [54,55]:

$$T(E) = Tr[\Gamma_{ee}^L G_{ee}^r \Gamma_{ee}^R G_{ee}^a],$$

$$T_{\text{AR}}(E) = Tr[\Gamma_{ee}^L G_{eh}^r \Gamma_{hh}^L G_{he}^a],$$

$$T_{\text{CAR}}(E) = Tr[\Gamma_{ee}^L G_{eh}^r \Gamma_{hh}^R G_{he}^a]. \quad (7)$$

Topological quantum phases play an important role in quantum transport, so determining the phase of the system is extremely important. Since topological invariants can change with closing the bulk gap, by solving the eigenvalues of the Hamiltonian $H_{\text{TSC}}$ in equation (3) and considering the gapless regions in the energy spectrum, one can obtain the following critical condition

$$m < -\sqrt{\Delta^2 + \mu^2} \quad \mathcal{N} = 2,$$
$$-\sqrt{\Delta^2 + \mu^2} < m < \sqrt{\Delta^2 + \mu^2} \quad \mathcal{N} = 1,$$
$$m > \sqrt{\Delta^2 + \mu^2} \quad \mathcal{N} = 0. \quad (8)$$

According to equation (8), the phase diagram of TSC can be mapped. Figure 1(b) shows the phase diagram in $(\Delta, m)$ plane with chemical potential $\mu = 0$ in the central TSC region. It can be seen from equation (8) that the three quantities ($m$, $\Delta$, and $\mu$) determine the quantum phase of the system, a change for any three quantities that may induce topological quantum phase transition of the system.

Due to inevitable defects in manufacturing processes, usually disorder also plays an important role in the quantum transport properties of the devices being studied. Based on the effective-medium theory, Groth $et\ al.$ discovered that Anderson disorder can induce self energy which causes a definite momentum state to decay exponentially as a function of time and space [36]. They also concluded that increasing the Anderson disorder strength can lead to a transition of topological mass $m$ from positive to negative. We replace the Hamiltonian of the TI in the central region with the TSC Hamiltonian; then the self-energy can be given by

$$[E_F + i0^+ - H_{\text{TSC}}(k) - \Sigma]^{-1} = < [E_F - H(k)]^{-1} >,$$
$$(9)$$

where $H_{\text{TSC}}(k)$ is the lattice Hamiltonian of the clean system of central TSC region in $k$ space and $< ... >$ represents the disorder average. The self-energy induced by disorder can be obtained from [56,57]

$$\Sigma = \frac{N}{\Omega} \sum_k U(k)G(k)U(k), \quad (10)$$

where $U(k)$ is random potential of the interaction produced by impurities in $k$ space, $N$ is the total number of impurities, and $\Omega$ is the volume of the disordered TSC region. For Anderson disorder, under the basis of $\varphi_k = [c_\uparrow(k), c_\downarrow(k), c_\uparrow^+(k), c_\downarrow^+(k)]^T$, $U(k)$ can be expressed by $U(k) = U(\tau_z \otimes \sigma_0)$, and $G = (E_F + i0^+ - H_{TSC}(k) - \Sigma)^{-1}$ is Green's function with disorder. The average strength of the disorder in equation (10) can be obtained by $\overline{U^2} = \frac{1}{WN} \int_{-\frac{W}{2}}^{\frac{W}{2}} U^2 dU = \frac{W^2}{12N}$. By using the self-consistent Born approximation, the self-energy induced by disorder in equation (10) can be concretely obtained from the integral equation [36,42]

$$\Sigma = \frac{W^2}{12}(\frac{1}{2\pi})^2 \int_{BZ} dk(\tau_z \otimes \sigma_0)$$
$$\times [E_F + i0^+ - H_{TSC}(k) - \Sigma]^{-1}(\tau_z \otimes \sigma_0), \quad (11)$$

where $BZ$ denote the integral over the first Brillouin zone. Self-energy $\Sigma$ can be decomposed with sixteen $4 \times 4$ Dirac matrices $\Sigma = \Sigma_0\gamma_0 + \Sigma_1\gamma_1 + \Sigma_2\gamma_2 + .... \Sigma_{15}\gamma_{15}$ where the fundamental Dirac matrices $\gamma_\mu$ can be expressed by $2 \times 2$ unit matrix $I$ and $2 \times 2$ Pauli's matrices $\sigma_j$, $\gamma_0 = \begin{pmatrix} I & 0 \\ 0 & I \end{pmatrix}$, $\gamma_j = \begin{pmatrix} 0 & -i\sigma_j \\ i\sigma_j & 0 \end{pmatrix}(j = 1, 2, 3)$, $\gamma_4 = \begin{pmatrix} I & 0 \\ 0 & -I \end{pmatrix}$, and the other eleven Dirac matrices can be obtained by $\gamma_5 = \gamma_1\gamma_2$, $\gamma_6 = \gamma_1\gamma_3$, $\gamma_7 = \gamma_1\gamma_4$, $\gamma_8 = \gamma_2\gamma_3$, $\gamma_9 = \gamma_2\gamma_4$, $\gamma_{10} = \gamma_3\gamma_4$, $\gamma_{11} = \gamma_2\gamma_3\gamma_4$, $\gamma_{12} = \gamma_3\gamma_4\gamma_1$, $\gamma_{13} = \gamma_4\gamma_1\gamma_2$, $\gamma_{14} = \gamma_1\gamma_2\gamma_3$, $\gamma_{15} = \gamma_1\gamma_2\gamma_3\gamma_4$ [58]. Therefore, the original Hamiltonian $H_{TSC}(k)$ is corrected and the topological mass is renormalized. The correction of topological mass is as follows

$$\overline{M} = M - \lim_{k \to 0} Im\Sigma_{13}. \quad (12)$$

## III. DISORDER INDUCED TOPOLOGICAL PHASE TRANSITION

In our numerical calculations, we set $A = B = 1$ and the lattice constant $a = 1$. We choose $m = -0.5$ in the two leads. The central TSC region size is fixed to $N_y = 100$ and $N_x = 60$. The incident electron energy is set to $E = 0$. The pair potential of the central TSC is fixed to $\Delta = 0.35$. The other parameters in central TSC region are fixed as follows unless otherwise specified: $\mu = 0$, $m = 0.45$. From equation (8), it can be deduced that the phases of the two leads are both in the QAHI phase [A point in Fig. 1(b)] where two degenerate chiral edge states present. While in TSC region $m = 0.45$ and $\Delta = 0.35$ [B point in Fig. 1(b)], the phase is in trivial phase with Chern number $\mathcal{N} = 0$. Therefore the energy gap presents around the Fermi energy, and an electron is restricted inside the energy gap. Due to that the length of the central TSC region is long enough to shut down both the electron and hole channel, none of the transmission processes can happen.

We wonder whether the disorder will affect the transport process of the proposed system. Thus, in Fig. 2(a), we calculate the normal tunneling coefficient $T$, the local Andreev reflection coefficient $T_{AR}$, and the crossed Andreev reflection coefficient $T_{CAR}$ through the hybrid system with the change of disorder strength $W$. In the simulation, random values of $w_i$ were used to calculate the conductance for 1000 times. The sum of the 1000 results is averaged. The three coefficients
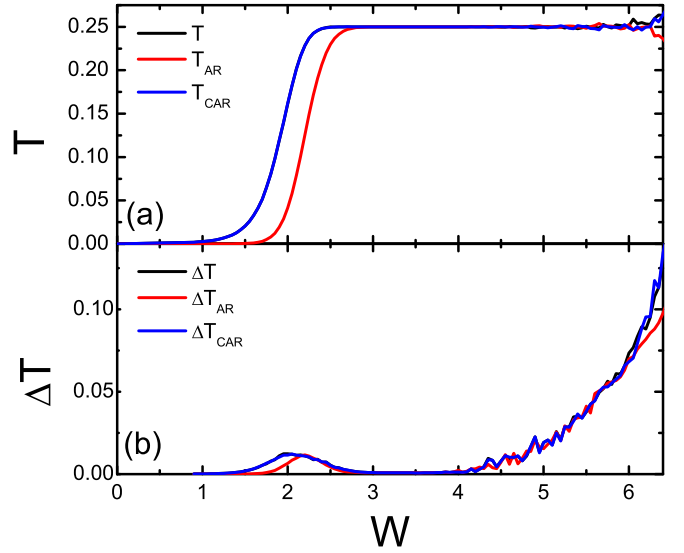


FIG. 2. (a) The normal tunneling coefficient $T$, the local Andreev reflection coefficient $T_{AR}$, and the crossed Andreev reflection coefficient $T_{CAR}$ as a function of disorder strength with $E = 0$, we choose $\mu = 0$, $m = 0.45$ and $\Delta = 0.35$ in the central TSC region, the length of the central TSC region is $N_x = 60$, the width of the central TSC region is $N_y = 100$, and we set $m = -0.5$ in the two leads. (b) The corresponding transmission coefficient fluctuation as a function of disorder strength. Here, the curves are averaged over results obtained with 1000 random values of $W$.

$T$, $T_{AR}$, and $T_{CAR}$ in Figs. 2(a) and 2(b) are represented by a black, red, and blue solid line, respectively. One can see from Fig. 2(a), just as expected, all three coefficients are zero with low disorder strength. But to our surprise, with the increase of disorder, the electron and copper pair transport through the junction with the same probability. We can see from Fig. 2(a) that the three coefficients increase to a plateau with a value of 0.25 around $W = 2$. Then the value of the plateau remains at 0.25 in a wide range of disorder strength until near $W = 5$. When $W > 5$, the other striking feature in Fig. 2(a) is present. That is, the coefficients show damped oscillatory behavior. Subsequently all three coefficients oscillate violently as the disorder strength increases. The change of the three coefficients plateau always implies a new phase. So we deduce that the quantum transition occurs near $W = 2$ and $W = 5$. We also study the fluctuation of the three coefficients $\Delta T = \sqrt{< T - < T \gg^2}$ where $< ... >$ represents the average over the disorder with the same disorder strength $W$ [29]. In Fig. 2(b), we plot the transmission coefficient fluctuations versus the disorder strength. $\Delta T$, $\Delta T_{AR}$, and $\Delta T_{CAR}$ represent the fluctuation of $T$, $T_{AR}$, and $T_{CAR}$ correspondingly. Figure 2(b) shows that with small $W$, there is no fluctuation. As disorder strength increases, the topological quantum phase transition occurs, so the fluctuations of the three coefficients emerge. As disorder strength continues to increase, the system is in a new topological phase. Thus, the fluctuations of the coefficients go to zero. When $m$ increases to around 4, the fluctuations emerge again. Thereafter the fluctuations show a trend of continuous increase. It indicates that the system undergoes another phase transition. The phenomena presented
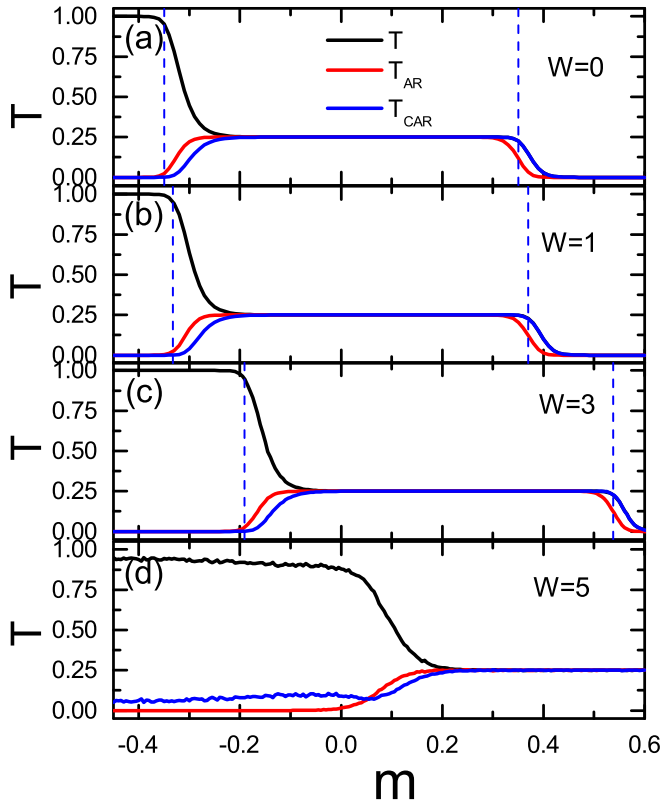
FIG. 3. The three coefficients $T$, $T_{AR}$, and $T_{CAR}$ as a function of topological mass $m$ with different disorder strength with (a) $W = 0$, (b) $W = 1$, (c) $W = 3$, and (d) $W = 5$. The vertical blue dashed lines in (a)–(c) are the boundaries of the TSC phases, which are $\mathcal{N} = 2$ to $\mathcal{N} = 1$ and $\mathcal{N} = 1$ to $\mathcal{N} = 0$, respectively. All of the curves are averaged over results obtained with 1000 random values of $W$. The other parameters are the same as for Fig. 2(a).



FIG. 4. The three coefficients $T$, $T_{AR}$, and $T_{CAR}$ as a function of chemical potential $\mu$ in the central TSC region for different disorder strength with (a) $W = 0$, (b) $W = 1$, (c) $W = 2$, and (d) $W = 3$. All of the curves are averaged over results obtained with 1000 random values of $W$. The other parameters are the same as for Fig. 2(a).

in Fig. 2(b) are consistent with the phenomena presented in Fig. 2(a).

In order to confirm whether the quantum phase transition really occurs with increasing of disorder strength in the central TSC region, we calculate the three coefficients $T$, $T_{AR}$, and $T_{CAR}$ through the hybrid system versus topological mass in the central TSC region for different disorder strengths with $W = 0$, 1, 3, 5, as shown in Figs. 3(a)–3(d). The sharpness of the slopes between the two conductance plateaus in Figs. 3(a)–3(d)) depends on the width of the system. To avoid large consumption of computing resources, we choose $N_y = 100$ and $N_x = 60$ in the simulations. Such parameters are sufficient to compare the boundaries of each TSC phase indicated by the blue dashed lines in Figs. 3(a)–3(c). We can see from Fig. 3(a) that when $m$ is less than $-0.35$, both $T_{AR}$ and $T_{CAR}$ are zero but $T$ presents a quantized plateau with a value of integer 1. It is mainly due to the fact that the formula in equation (8) $m < -\sqrt{\Delta^2 + \mu^2}$ is satisfied; the system is in the topological phase of $\mathcal{N} = 2$, as shown in Fig. 1(b) within the pink region, thus the edge current is perfectly transmitted [16]. When $m$ is between $-0.35$ and 0.35, corresponding with the blue region in Fig. 1(b) where the condition $-\sqrt{\Delta^2 + \mu^2} < m < \sqrt{\Delta^2 + \mu^2}$ is satisfied. The TSC phase transits from
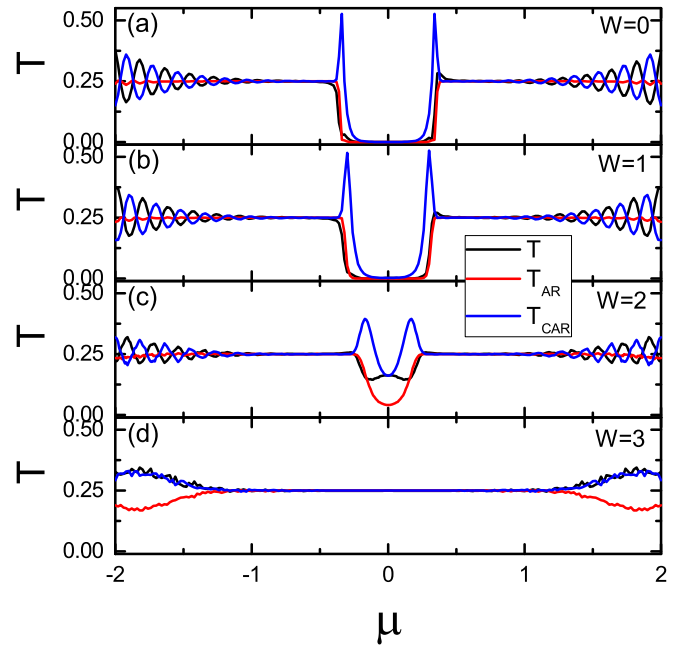
$\mathcal{N} = 2$ to $\mathcal{N} = 1$, and there only exists one chiral Majorana edge state in the central TSC region, so the four scattering processes—electron tunneling, normal reflection, the Andreev reflection, and the crossed Andreev reflection—have equal probability with a value of 1/4 fraction [16,18,21]. When $m > 0.35$, the condition $m > \sqrt{\Delta^2 + \mu^2}$ is satisfied, and the TSC phase transits from the $\mathcal{N} = 1$ nontrivial state to the trivial state with Chern number $\mathcal{N} = 0$. For the $W = 1$ case, as shown in Fig. 3(b), compared with Fig. 3(a), the entire image has only a slight offset to the right. It implies that the three coefficients have not undergone conspicuous changes. Such a result is consistent with those of other researches, which indicates that the nontrivial state is robust against weak disorder [17,59]. For the $W = 3$ case, the three coefficients show obvious right offset, as clearly shown in Fig. 3(c). But the two conductance plateaus are still maintained. For the $W = 5$ case, we can see clearly in Fig. 3(d) that the plateau of $\mathcal{N} = 2$ is destroyed, but the plateau $\mathcal{N} = 1$ remains and it still shifts rightward. From the above analysis we can conclude that the phase corresponding with $m = 0.45$ in the central TSC region does undergo phase transition.

We have demonstrated that the phase transitions happen with increasing of disorder strength in the central TSC region. Next, we focus attention on the three coefficients through the hybrid system with the changes of chemical potential in the central TSC region where the disorder strength $W = 0$, 1, 2, and 3 is considered, as shown in Figs. 4(a)–4(d), respectively. Here, we fix $m = 0.45$ and $\Delta = 0.35$ in the central TSC region. One can find that, in Fig. 4(a), three coefficients $T$, $T_{AR}$, and $T_{CAR}$ are completely equal to zero, as long as the chemical potential lies inside a certain range. The reason is that in this
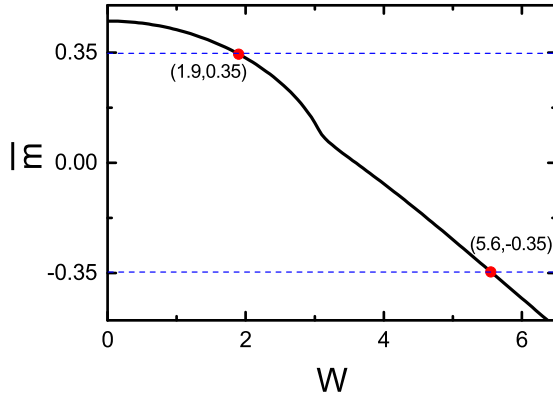
FIG. 5. The renormalized topological mass $\overline{m}$ vs disorder strength $W$. The blue dashed lines represent the critical phase boundaries where renormalized topological mass correspond to $\overline{m} = -0.35$ and $\overline{m} = 0.35$. The critical phase transition points are represented by the red solid dot. The other parameters are the same as in Fig. 2(a).
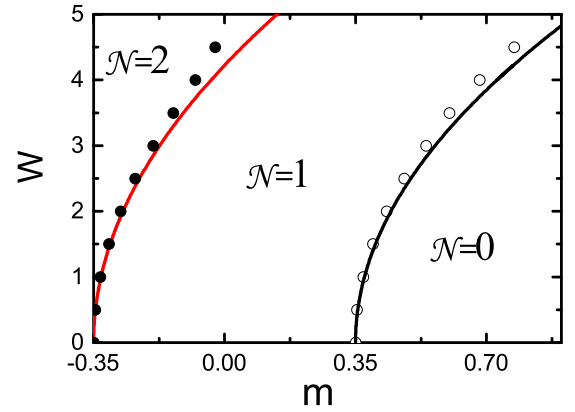


FIG. 6. Phase diagram of the $(W, m)$ plane. The black solid line and the red solid line correspond to the quantum phase transition boundary of the renormalized topological mass term which is calculated by the effective-medium theory with $\overline{m} = -0.35$ and $\overline{m} = 0.35$, respectively. The black open circles and black solid dots are the results of two critical boundaries calculated by transport theory. $\mathcal{N}$ labels the Chern number of the TSC. The other parameters are the same as in Fig. 2(a).

range, although the chemical potential changes, the condition $m > \sqrt{\Delta^2 + \mu^2}$ is still satisfied, so the phase of the TSC central region is at trivial phase with Chern number $\mathcal{N} = 0$, and none of the transmission processes can happen. When the chemical potential deviates from this range, the nontrivial phase with Chern number $\mathcal{N} = 1$ is realized, thus the three coefficients $T$, $T_{AR}$, and $T_{CAR}$ are fixed to the plateau with a value of $1/4$. When the deviation is further increased, $T$, $T_{AR}$, and $T_{CAR}$ present damped oscillation behaviors around the value $1/4$. We can see clearly from Figs. 4(b) and 4(c) that with the increase of the disorder strength, the interval of trivial TSC is significantly narrower; at last in Fig. 4(d) the interval of the trivial TSC disappeared, but the condition $m > \sqrt{\Delta^2 + \mu^2}$ is still satisfied. The phenomenon shown in Figs. 4(b)–4(d) is confusing. Fortunately, based on the effective-medium theory, Groth *et al.* found that the Anderson disorder can make a negative correction to the topological mass $m$ in 2D TI HgTe [36]. Thus, they theoretically explain the topological quantum phase transition in TI induced by Anderson disorder. However, whether this theory can explain the quantum transition of TSC and reveal its physical mechanism is still questionable.

## IV. MECHANISM AND EXPLANATION OF THE TOPOLOGICAL PHASE TRANSITION

In order to solve the above doubts, in Fig. 5, we use the effective-medium theory to numerically calculate the renormalized topological mass $\overline{m}$ as a function of the disorder strength $W$ at incident electron energy $E = 0$, where the TSC with chemical potential $\mu = 0$ is considered. One can see that, as expected, the renormalized topological mass term $\overline{m}$ decreases monotonously with the increase of disorder $W$. We also give the boundaries of the topological quantum phase transition from Chern number $\mathcal{N} = 0$ to $\mathcal{N} = 1$ and from $\mathcal{N} = 1$ to $\mathcal{N} = 2$, as shown by the blue dashed line in Fig. 5. We notice that the critical phase transition points with $\overline{m} = -0.35$ and $\overline{m} = 0.35$ are at $W = 1.9$ and $W = 5.6$, respectively. The result is consistent with the position where the plateau begins and where the oscillation starts to emerge in Fig. 2(a).

To see this more clearly, we also plot a phase diagram in the $(W, m)$ plane by using the effective-medium theory as shown in Fig. 6. In Fig. 6, the critical quantum phase boundary which corresponds to renormalized mass $\overline{m} = 0.35$ is indicated by the black solid line. The red solid line represents the critical phase boundary which corresponds to renormalized mass $\overline{m} = -0.35$. Therefore, the topological phases of $\mathcal{N} = 0, 1, 2$ can be clearly distinguished. To quantitatively test the phase diagram resulting from the effective-medium theory, we use the results of numerical transport simulations in Fig. 3 (The cases with $W = 0.5, 1.5, 2.0, 2.5, 3.5, 4.5$ are not given in this paper). The critical quantum phase boundaries for $\mathcal{N} = 0$ to $\mathcal{N} = 1$ and $\mathcal{N} = 1$ to $\mathcal{N} = 2$ shown in Fig. 3 are represented by the hollow circles and solid dots, respectively. We can see from Fig. 6 that for weak disorder, the numerical transport simulation results are consistent with the results of the effective-medium theory, but for strong disorder strength there are deviations of both cases. The reason is that the effective-medium theory is only applicable for weak disorder [36].

In order to get the whole phase diagram in the $(W, m)$ plane, we calculate transmission coefficient $T$ again using transport theory. In our calculation, 300 random values of $W$ were used to calculate the transmission coefficient. In Fig. 7, $\mathcal{N} = 0, 1$, and 2 phases are represented by blue, green, and sauce red region, respectively. By comparing with Fig. 6, we find that for weak Anderson disorder strength the phase diagram is consistent with that of Fig. 6. It can be seen as well from Fig. 7 that when disorder strength $W = 7.5$ the two boundary lines intersect at one point. One can also notice that in Fig. 7, when the disorder strength $W > 12.5$, the phase of the system is stable at the $\mathcal{N} = 0$ phase, regardless of the value of the topological mass $m$. This is consistent with the common sense of physics, that is, too heavy doping destroys the edge state completely, and the central region becomes an insulator with Chern number $\mathcal{N} = 0$.
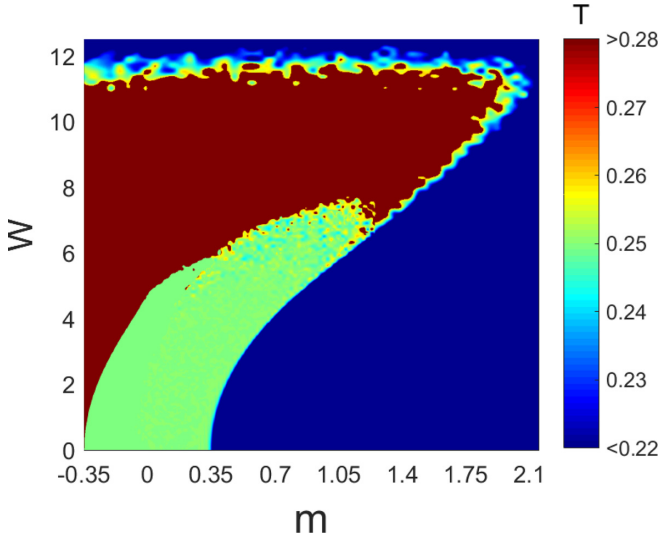
FIG. 7. Simulation of topological quantum phases, showing the average transmission coefficient $T$ as a function of disorder strength $W$ and topological mass $m$. All points are averaged over results obtained with 300 random values of $W$. The other parameters are the same as Fig. 2(a).

Finally, we discuss the actual parameters of our dimensionless model. Majorana fermions are experimentally discovered in Cr-(Bi, Sb)$_2$Te$_3$ coupled superconductor film [23]. By comparing the model spectrum with density functional theory band structures of Bi$_2$Se$_3$ thin films, Zeng *et al.* roughly estimated the actual parameters of topological mass and pairing potential; they found that the two parameters are of the order of 1 meV [60]. In addition, the proximity induced superconductor gap of the Bi$_2$Se$_3$ film grown on the NbSe$_2$ substrate can even reach 1.1 meV at 4.2 K and can be tuned by the thickness of the film [61]. This means that the pair potential can be modulated in a certain energy range. Recently, by analyzing and comparing experimental results, Yan *et al.* gave the actual values of the parameters of the model [62]. Since we use the same model and a similar structure as theirs, the actual parameters used in our simulation correspond to actual

parameters $m = 0.45$ meV and $\Delta = 0.35$ meV. Therefore, it can be concluded that when disorder strength $W > 1$ meV, the conductance plateaus can be tuned conspicuously in experiment.

## V. CONCLUSIONS

In summary, we have studied the Anderson disorder effects on transport properties in the QAHI/trivial TSC/QAHI hybrid system. We find that with increasing of Anderson disorder strength the conductance plateaus exhibit the characteristics of parallel offset; we deduce that Anderson disorder can drive a trivial phase in the central region into a chiral TSC phase. Next, based on the effective-medium theory, we find that the Anderson disorder can make a negative correction to the topological mass $m$. We also find that with increasing of disorder strength, the renormalized topological mass monotonously decreases. Therefore, it can induce transition from a trivial phase with $\mathcal{N} = 0$ to a nontrivial phase. Subsequently, numerically comparing our transport results with the results of the effective-medium theory, we find that with weak disorder strength, the results of the two calculations are completely consistent, however, because the effective-medium theory is only applicable for weak disorder, for strong disorder there are deviations. In addition, by using the transport theory, the entire phase diagrams are obtained. Thus we point out the region for obtaining chiral Majorana edge states with Chern number $\mathcal{N} = 1$. At last, we conclude that the results not only further verify the availability of the effective medium theory in disordered TSC but also are important for realization of the chiral TSC phase in experiment with Anderson disorder.

[1] E. Majorana, Nuovo Cimento **14**, 171 (1937).

[2] M. H. Freedman, Proc. Natl. Acad. Sci. **95**, 98 (1998).

[3] A. Yu. Kitaev, Ann. Phys. **303**, 2 (2003).

[4] J. Alicea, Y. Oreg, G. Refael, F. V. Oppen, and M. P. A. Fisher, Nat. Phys. **7**, 412 (2011)

[5] C. Nayak, S. H. Simon, A. Stern, M. Freedman, and S. Das Sarma, Rev. Mod. Phys. **80**, 1083 (2008).

[6] X. L. Qi and S. C. Zhang, Rev. Mod. Phys. **83**, 1057 (2011).

[7] J. Alicea, Rep. Prog. Phys. **75**, 076501 (2012).

[8] C. W. J. Beenakker, Annu. Rev. Condens. Matter Phys. **4**, 113 (2013).

[9] G. Moore and N. Read, Nucl. Phys. B **360**, 362 (1991).

[10] N. Read and E. Rezayi, Phys. Rev. B **59**, 8084 (1999).

[11] N. Read and D. Green, Phys. Rev. B **61**, 10267 (2000).

[12] A. Yu. Kitaev, Phys. Usp. **44**, 131 (2001).

[13] L. Fu and C. L. Kane, Phys. Rev. Lett. **100**, 096407 (2008).

[14] L. Fu and C. L. Kane, Phys. Rev. B **79**, 161408(R) (2009).

[15] X. L. Qi, T. L. Hughes, and S. C. Zhang, Phys. Rev. B **82**, 184516 (2010).

[16] Y. T. Zhang, Z. Hou, X. C. Xie, and Q. F. Sun, Phys. Rev. B **95**, 245433 (2017).

[17] Y. T. Zhang, X. Deng, Q. F. Sun, and Z. H. Qiao, Sci. Rep. **5**, 14892 (2015).

[18] H. B. Wu, Y. T. Zhang, and J. J. Liu, J. Appl. Phys. **124**, 084301 (2018).

[19] J. J. He, J. Wu, T. P. Choy, X. Jun Liu, Y. Tanaka, and K. T. Law, Nat. Commun. **5**, 3232 (2014).

[20] Y. H. Li, J. Liu, H. W. Liu, H. Jiang, Q. F. Sun, and X. C. Xie, Phys. Rev. B **98**, 045141 (2018).

[21] S. B. Chung, X. L. Qi, J. Maciejko, and S. C. Zhang, Phys. Rev. B **83**, 100512(R) (2011).

[22] J. Wang, Q. Zhou, B. Lian, and S. C. Zhang, Phys. Rev. B **92**, 064520 (2015).

[23] Q. L. He, L. Pan, A. L. Stern, E. C. Burks, X. Che, G. Yin, J. Wang, B. Lian, Q. Zhou, E. S. Choi, K. Murata, X. Kou, Z. Chen, T. Nie, Q. Shao, Y. Fan, S.-C. Zhang, K. Liu, J. Xia, and K. L. Wang, Science **357**, 294 (2017).

[24] W. Ji and X. G. Wen, Phys. Rev. Lett. **120**, 107002 (2018).

[25] Y. Huang, F. Setiawan, and J. D. Sau, Phys. Rev. B **97**, 100501(R) (2018).

[26] A. Kapitulnik, N. Mason, S. A. Kivelson, and S. Chakravarty, Phys. Rev. B **63**, 125322(R) (2001).

[27] B. Lian, J. Wang, X. Q. Sun, A. Vaezi, and S. C. Zhang, Phys. Rev. B **97**, 125408 (2018).

[28] M. Kayyalha, D. Xiao, R. X. Zhang, J. Shin, J. Jiang, F. Wang, Y.-F. Zhao, R. Xiao, L. Zhang, K. M. Fijalkowski, P. Mandal, M. Winnerlein, C. Gould, Q. Li, L. W. Molenkamp, M. H. W. Chan, N. Samarth, and C.-Z. Chang, Science **367**, 64 (2020).

[29] W. Long, Q. F. Sun, and J. Wang, Phys. Rev. Lett. **101**, 166806 (2008).

[30] Y. Y. Zhang and S. Q. Shen, Phys. Rev. B **88**, 195145 (2013).

[31] Y. Y. Zhang, M. Shen, X. T. An, Q. F. Sun, X. C. Xie, K. Chang, and S. S. Li, Phys. Rev. B **90**, 054205 (2014).

[32] H. B. Wu, Y. T. Zhang, and J. J. Liu, J. Appl. Phys. **121**, 094306 (2017).

[33] J. Lu, B. Xi, and M. Li, New J. Phys. **20**, 083017 (2018).

[34] H. Jiang, L. Wang, Q. F. Sun, and X. C. Xie, Phys. Rev. B **80**, 165316 (2009).

[35] J. Li, R. L. Chu, J. K. Jain, and S. Q. Shen, Phys. Rev. Lett. **102**, 136806 (2009).

[36] C. W. Groth, M. Wimmer, A. R. Akhmerov, J. Tworzydło, and C. W. J. Beenakker, Phys. Rev. Lett. **103**, 196805 (2009).

[37] J. T Song, H. W. Liu, H. Jiang, Q. F. Sun, and X. C. Xie, Phys. Rev. B **85**, 195125 (2012).

[38] H. M. Guo, G. Rosenberg, G. Refael, and M. Franz, Phys. Rev. Lett. **105**, 216601 (2010).

[39] D. F. Mross, Y. Oreg, A. Stern, G. Margalit, and M. Heiblum, Phys. Rev. Lett. **121**, 026801 (2018).

[40] C. Wang, A. Vishwanath, and B. I. Halperin, Phys. Rev. B **98**, 045112 (2018).

[41] S. Ryu and K. Nomura, Phys. Rev. B **85**, 155138 (2012).

[42] J. Borchmann, A. Farrell, and T. Pereg-Barnea, Phys. Rev. B **93**, 125133 (2016).

[43] C. B. Hua, R. Chen, D. H. Xu, and B. Zhou, Phys. Rev. B **100**, 205302 (2019).

[44] W. Qin, D. Xiao, K. Chang, S. Q. Shen, and Z. Y. Zhang, Sci. Rep. **6**, 39188 (2016).

[45] R. Yu, W. Zhang, H. Zhang, S. Zhang, X. Dai, and Z. Fang, Science **329**, 61 (2010).

[46] X. L. Qi, Y. S. Wu, and S. C. Zhang, Phys. Rev. B **74**, 085308 (2006).

[47] P. W. Anderson, Phys. Rev. **109**, 1492 (1958).

[48] Y. Meir and N. S. Wingreen, Phys. Rev. Lett. **68**, 2512 (1992).

[49] A. P. Jauho, N. S. Wingreen, and Y. Meir, Phys. Rev. B **50**, 5528 (1994).

[50] S. Datta, *Quantum Transport: Atom to Transistor* (Cambridge University Press, Cambridge, 2005).

[51] D. H. Lee and J. D. Joannopoulos, Phys. Rev. B **23**, 4997 (1981).

[52] M. P. L. Sancho, J. M. L. Sancho, and J. Rubio, J. Phys. F: Met. Phys. **14**, 1205 (1984).

[53] M. P. L. Sancho, J. M. L. Sancho, and J. Rubio, J. Phys. F: Met. Phys. **15**, 851 (1985).

[54] Q. F. Sun and X. C. Xie, J. Phys.: Condens. Matter **21**, 344204 (2009).

[55] S. G. Cheng, Y. Xing, J. Wang, and Q.-F. Sun, Phys. Rev. Lett. **103**, 167003 (2009).

[56] D. K. Ferry, and S. M. Goodnick, *Transport in Nanostructures* (Cambridge University Press, England, 1997).

[57] S. Doniach, and E. H. Sondheimer, *Green's Functions for Solid State Physicists* (World Scientific, Singapore, 1998).

[58] R. H. GooD, Jr., Rev. Mod. Phys. **27**, 187 (1955).

[59] M. Wei, M. Zhou, Y. T. Zhang, and Y. Xing, Phys. Rev. B **101**, 155408 (2020).

[60] Y. X. Zeng, C. Lei, G. Chaudhary, and A. H. MacDonald, Phys. Rev. B **97**, 081102(R) (2018).

[61] M.-X. Wang, C. Liu, J.-P. Xu, F. Yang, L. Miao, M.-Y. Yao, C. L. Gao, C. Shen, X. Ma, X. Chen, Z.-A. Xu, Y. Liu, S.-C. Zhang, D. Qian, J.-F. Jia, and Q.-K. Xue, Science **336**, 52 (2012).

[62] Q. Yan, Y. F. Zhou, and Q. F. Sun, Phys. Rev. B **100**, 235407 (2019).